Electronic Supplementary Material (ESI) for Nanoscale.

Thermal rectification at bimaterial nanocontact interface

Zhen-Qiang Ye[1], *Bing-Yang Cao*[1,*]

[1]Key Laboratory for Thermal Science and Power Engineering of Ministry of Education, Department of Engineering Mechanics, Tsinghua University, Beijing 100084, P. R. China

[*]Electronic mail: caoby@tsinghua.edu.cn, Tel/Fax: +86-10-6279-4531.

Supplementary Information

Supplementary Note 1: Experimental method

The circuit mainly consists of a heating beam and a sensing beam, which are placed in a high vacuum cryostat. Fig. S1 is the schematic diagram of the method. It shows that a 1-ω AC current is applied on the heating beam and a DC current is on the sensing beam. The heating power is a 2-ω signal, so the temperature rise is a 2-ω signal too. The resistance rise is proportional to the temperature rise. Considering the current, we can get 3-ω and 2-ω voltage changes for the heating beam and the sensing beam, respectively, to estimate their temperature rises.

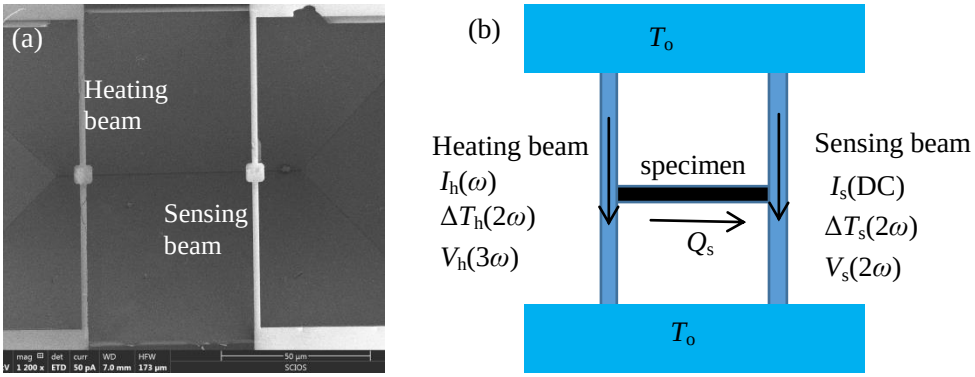

Figure S1. (a) SEM image of the fabricated suspended device; (b) the circuit schematic diagram of AC method.

The heat flux in the sensing beam, Q_s, is equal to that in the specimen, so we can get the relation between the thermal conductance of specimen, G_{sp}, and the heat flux Q_s ,

$$Q_s = G_{sp}(\Delta T_h - \Delta T_s), \quad (1)$$

in which ΔT_h and ΔT_s are the central temperature rises of the heating beam and the sensing beam, respectively. In addition, the heat transfer in the sensing beam can be expressed as

$$Q_s = G_s \Delta T_s , \tag{2}$$

in which G_s is the central thermal conductance of the sensing beam. So, the thermal conductance of the specimen is

$$G_{sp} = G_s \frac{\Delta T_s}{(\Delta T_h - \Delta T_s)}, \tag{3}$$

For the heating side, the temperature rise and the 3-ω voltage are related as

$$\Delta T_h = \frac{3V_{h,3\omega}}{I_h} (\frac{dR_h}{dT})^{-1}, \tag{4}$$

where $\frac{dR_h}{dT}$ is proportional to the temperature coefficient of resistance (TCR),

$$\text{TCR} = \frac{1}{R_0} (\frac{dR_h}{dT}), \tag{5}$$

The central thermal conductance of the heating beam is

$$G_h = \frac{Q_h}{2\Delta T_h}, \tag{6}$$

where Q_h refers to the heating power applied on the heating beam. We make an assumption that the thermal conductance of the sensing beam, G_s, is equal to G_h, since they are made of the same material, and G_s cannot be directly obtained through the first measurement. A full Wheatstone bridge is employed to measure the 2-ω voltage of the sensing side as shown in Fig. S2. The temperature rise of the sensing side is given as

$$\Delta T_s = 2\overline{dT_s} = \frac{2\sqrt{2}V_{s,2\omega}(R_s + R_1 + R_{s,p} + R_2)}{I_{s,DC}(\mathrm{d}R_s / \mathrm{d}T)R_2}. \tag{7}$$

For convenience, S_h, S_s and R_{tot} are short for $\mathrm{d}R_h/\mathrm{d}T$, $\mathrm{d}R_s/\mathrm{d}T$ and $(R_s+R_1+R_2+R_{s,p})$, respectively, in the following sections.

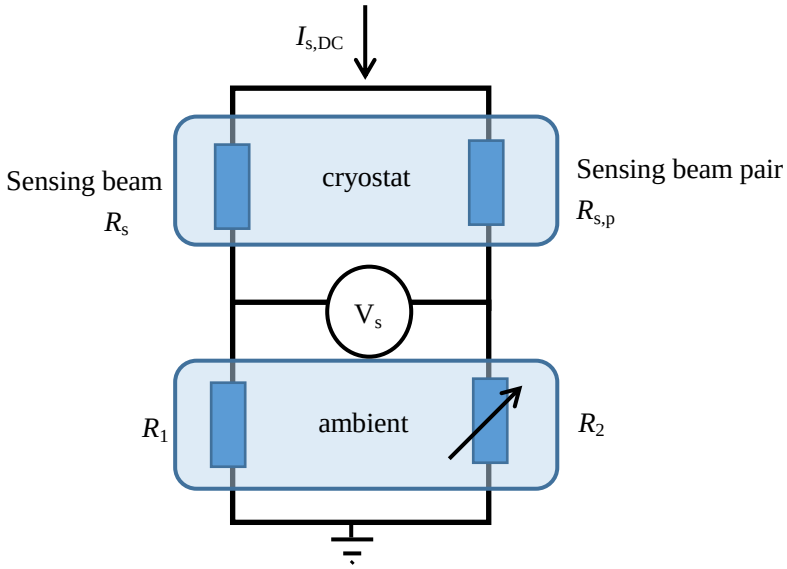

Figure S2. The Wheatstone bridge used for the sensing beam to measure the temperature rise.

Supplementary Note 2: Uncertainty analysis

Analysis of measurement uncertainty is necessary for the experimental reliability. For the case $\Delta T_h >> \Delta T_s$, the uncertainty of the measured sample can be written as

$$\frac{\delta(G_{sp})}{G_{sp}} = \frac{\delta(Q_h)}{Q_h} + \frac{\delta(T_s)}{T_s} + \frac{2\delta(T_h)}{T_h}. \tag{8}$$

According to Eqs. (3-7), the three parts can be expressed as

$$\frac{\delta(Q_h)}{Q_h} = \frac{2\delta(I_h)}{I_h} + \frac{\delta(R_h)}{R_h}; \tag{9}$$

$$\frac{\delta(\Delta T_h)}{\Delta T_h} = \frac{2\delta(V_{h,3\omega})}{V_{h,3\omega}} + \frac{\delta(I_h)}{I_h} + \frac{\delta(S_h)}{S_h}; \tag{10}$$

$$\frac{\delta(\Delta T_s)}{\Delta T_s} = \frac{2\delta(V_{s,2\omega})}{V_{s,2\omega}} + \frac{\delta(I_{s,\mathrm{dc}})}{I_{s,\mathrm{dc}}} + \frac{\delta(S_s)}{S_s}. \tag{11}$$

For the first part, the measurement uncertainty of I_h and R_h are negligible (less than 0.1%). For the second part, only $\delta(S_h)$ is mattered. By fitting the curves in Fig.4d, we get the slope and TCR, as

shown in Tab. S1. According to Tab. S1, $\delta(S_h)/S_h$=0.343%. The third part depends on $\delta(S_s)$, and $\delta(S_s)/S_s$=0.388%. We get $\delta(G_{sp})/G_{sp}$=1.07%. In general, the uncertainty of the experiments is small than thermal rectification ratio, so the thermal rectification of our experiments is authentic.

Table S1. TCR of heating beam and sensing beam.

	$\frac{dR}{dT}$ [Ω/K]	Standard error [Ω/K]	TCR [1/K]
Heating beam	1.3970	0.00480	0.001405
Sensing beam	1.4025	0.00548	0.001402

Supplementary Note 3: Potential verification and the influence of size effect

The potential model for PA-11 consists of four parts, namely, bond constrains V_{bond}, angle bending V_{angle}, torsions V_{torsion} and nonbonded interactions V_{nb},

$$V = V_{\text{bond}} + V_{\text{angle}} + V_{\text{torsion}} + V_{\text{nb}}; \tag{12}$$

$$V_{\text{bond}} = \frac{1}{2} K_b (r - r_0)^2; \tag{13}$$

$$V_{\text{angle}} = \frac{1}{2} K_a (\varphi - \varphi_0)^2; \tag{14}$$

$$V_{\text{torsion}} = \frac{1}{2} \sum_n V_n \cos n\tau; \tag{15}$$

$$V_{\text{nb}} = \frac{q_i q_j}{4\pi\varepsilon_0} \left(\frac{1}{r_{ij}} + \frac{\varepsilon_{rf} - 1}{2\varepsilon_{rf} + 1} \frac{r_{ij}^2}{r_{cut}^3}\right) + 4\varepsilon_{ij} \left[\left(\frac{\sigma_{ij}}{r_{ij}}\right)^{12} - \left(\frac{\sigma_{ij}}{r_{ij}}\right)^6\right]. \tag{16}$$

Detailed parameters are provided in Ref. [14].

We simulate the thermal properties of PA nanowires and PA single chain based on the above potential, and the results are shown in Fig. S3. The single PA-11 chain has an extremely high length-dependent thermal conductivity, which increases from 16.8 W/(m·K) to 30.8 W/(m·K)

when the length increases from 10.2 nm to 42 nm at room temperature. The thermal conductivity increases monotonously with the increasing temperature ranging from 250 K to 400 K, while it drops dramatically with the increasing diameter. It is only 4.4 W/(m·K) for the nanowire with diameter of 1.02 nm at room temperature. Generally, the trend and the order of magnitudes of thermal conductivity are consistent with Ref. [43].

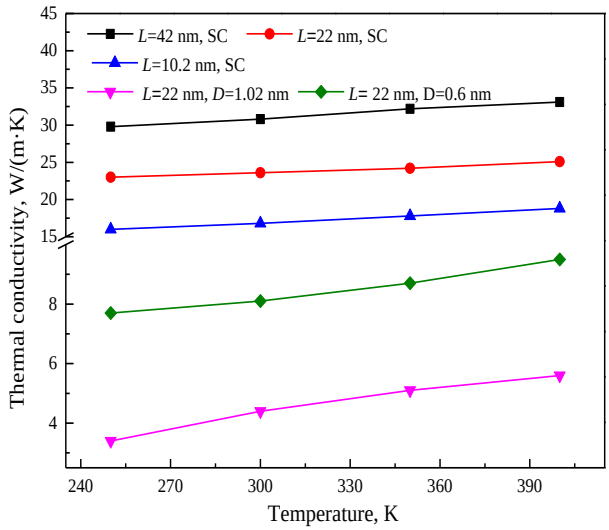

Figure S3. Thermal conductivities of PA nanowires and PA single chain.

Stillinger–Weber potential is used to generate Si nanowire, which is a many-body model including both the pair and triplet potentials,

$$V = \sum \frac{1}{2} V_{ij} + \sum \frac{1}{6} V_{ijk}\,; \tag{17}$$

$$V_{ij} = \varepsilon f_2(\frac{r_{ij}}{\sigma})\,; \tag{18}$$

$$f_2(r) = \begin{cases} A(Br^{-p} - r^{-q})\exp(r-a)^{-1}, & r < a \\ 0, & r \geq a \end{cases}; \tag{19}$$

$$V_{ijk} = \varepsilon f_3(\frac{r_i}{\sigma} + \frac{r_j}{\sigma} + \frac{r_k}{\sigma})\,; \tag{20}$$

$$f_3(r_i, r_j, r_k) = h(r_{ij}, r_{ik}, \theta_{jik}) + h(r_{ji}, r_{jk}, \theta_{ijk}) + h(r_{ki}, r_{kj}, \theta_{ikj}), \quad (21)$$

where *a* denotes the potential cutoff distance, *A*, *B*, *p* and *q* are all parameters. See Ref. [16] for the further details. The interaction between PA and Si is modeled by L-J potential.

$$V_{\mathrm{LJ}} = 4\varepsilon_{ij}[(\frac{\sigma_{ij}}{r_{ij}})^{12} - (\frac{\sigma_{ij}}{r_{ij}})^{6}] \quad (22)$$

.

The energy parameter ε and distance parameter σ are listed in Tab. S2, where Cn and Hn, respectively, denote the carbon and hydrogen atoms of amide group. Fig. S4 shows the structure of PA single chain, Si nanowire and PA/Si nanowires obtained by MD simulations. In short, the above potentials for PA and Si are reliable.

Table S2. Parameters describing the interaction between PA and Si.

	ε [kcal/mol]	σ [Å]
C-Si	1.0811	2.0600
Cn-Si	1.0606	2.0600
O-Si	1.0510	2.0600
N-Si	1.0258	1.8640
H-Si	1.0686	1.5140
Hn-Si	1.0686	1.5140

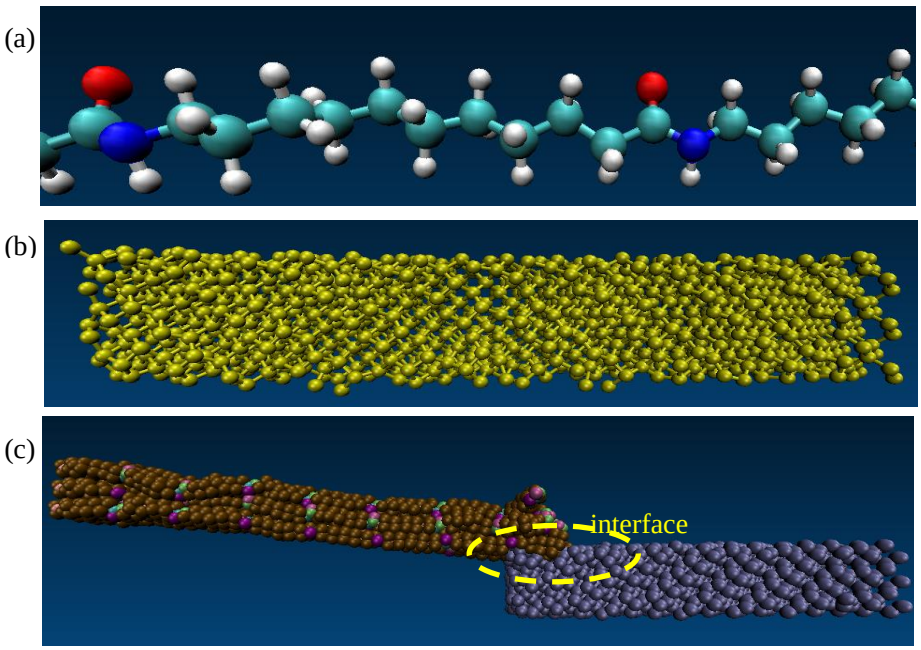

Figure S4. Schematic of (a) a single PA-11 chain, (b) Si nanowire and (c) PA/Si crossed nanowire.

To investigate the size effect in the direction of heat flux, we simulated another two cases. For case1, the length of PA is 22.8 nm, of silicon is 16.1 nm, and the overlap length is 4 nm; for case2, the length of PA is 30.5 nm, of silicon is 22.5 nm, and the overlap length is 4 nm. The simulation results are shown in Figure S5. It shows that Si→ PA still has higher thermal conductance for both cases. It is estimated that the rectification ratio is about 21.2% and 24.3% for case1 and case2, respectively, based on the slope of the curves. It should be emphasized that the thermal conductivity of the whole system increases with an increasing length. Compared with the results in Figure 5b, the thermal rectification ratio increases with the increasing system length. It is due to the interface plays more important role in a longer system if the overlap length remains unchanged. In a word, the size effect does not change the direction of thermal rectification.

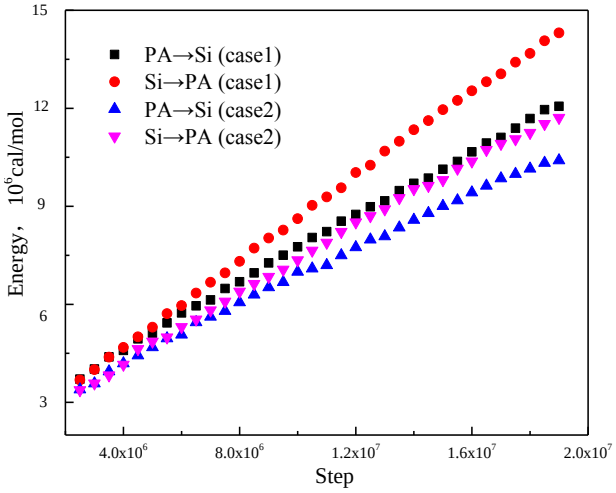

Figure S5. Energy accumulation of the thermostats of the two cases

Supplementary Note 4: Experiments of single PA nanofiber

We measure the temperature-dependent thermal conductance of two PA-11 nanofiber specimens. Fig. S6 gives the SEM images of the two specimens. The first specimen has a diameter of 870.4 ±11.74 nm, and the second one is 1380.75 ±26.3 nm.

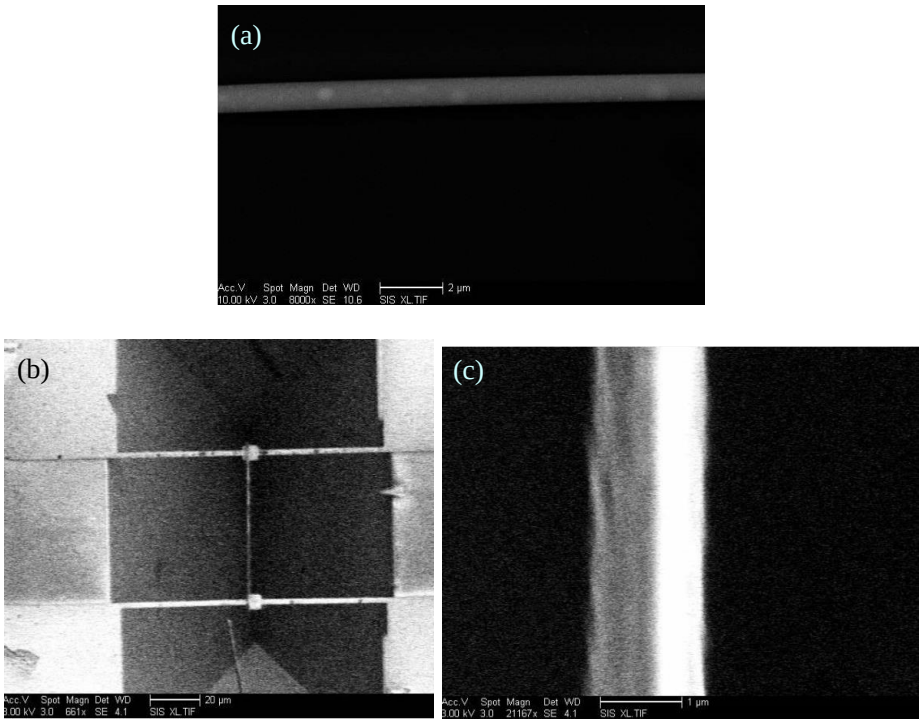

Figure S6. SEM images of (a) the first specimen (b) the second specimen, and (c) enlarged view of the second specimen.

The temperature-dependent thermal conductivities are shown in Fig. S7. Firstly, it shows that the thinner one has a much larger thermal conductivity than the thicker one, and both of them have higher thermal conductivities than that of bulk PA (0.216~0.24 W/(m·K) at room temperature). It is because the polymer chains with a thinner diameter have a better orientation and larger crystal domains, which can enhance the heat conduction. Secondly, the thermal conductivities of both increase with the increasing temperature. For the thinner one, the thermal conductivity rises by 35.2% as the temperature increases from 150 to 300 K. For the thicker one, the thermal conductivity rises by 57.1% as the temperature increases from 100 to 300 K.

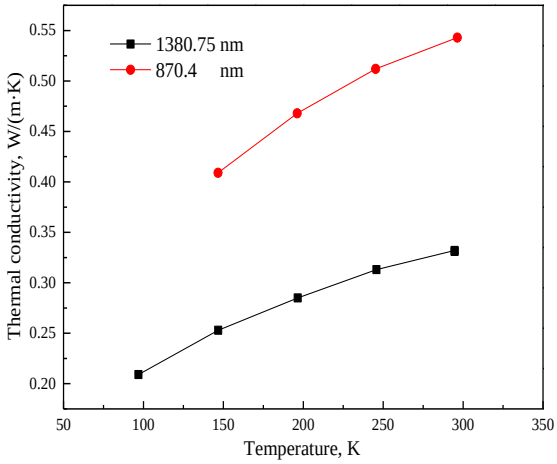

Figure S7. The temperature-dependent thermal conductivities of the specimens with diameters of 1380.75 nm and 870.4 nm.

Then, we check the repeatability, as shown in Fig. S8. It shows the measurement of the second sample at room temperature. We applied forward heat flux and backward heat flux, respectively, and each direction for twice. The slope of the curves can reflect the thermal conductance based on Eq. (3). It shows that the repeatability of the experiment is good, and it does

not show any thermal rectification in a single nylon.

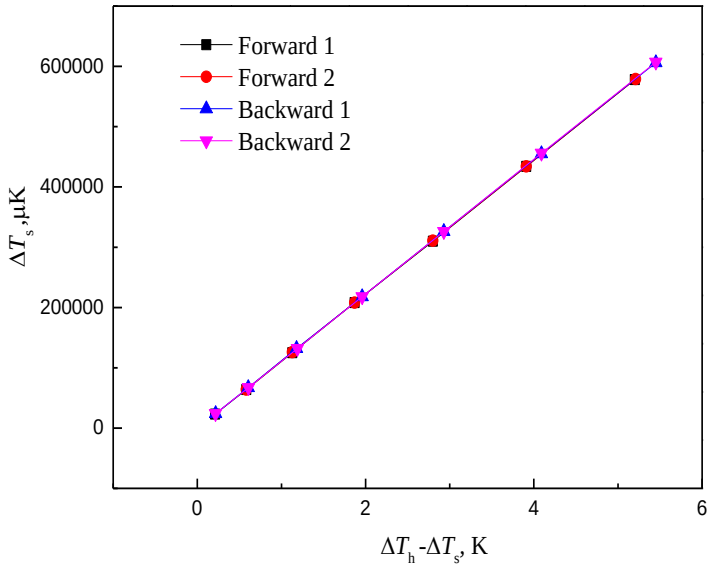

Figure S8. The measurement of the second single nylon at room temperature. The heating voltage ranges from 1 V to 5 V.

Supplementary Note 5: The influence of temperature-dependence of thermal conductance on thermal rectification

For the experiments, we find that the maximum temperature difference between the heating beam and the sensing beam is less than 5 K, which leads to far less than 1% change of thermal conductance, so we can neglect the temperature influence in experiments. Here, we only focus on the MD simulations. Fig. S9 gives the temperature-dependent thermal conductance of PA and Si by MD simulations. The initial length of PA is 100 Å, and of Si is 60 Å. Both of them have a diameter of about 15 Å. It shows that the thermal conductance of PA increases with the increasing temperature, which rises by 9% as the temperature increasing from 200 K to 400 K. The thermal conductance of the Si nanowire decreases with the increasing temperature, which drops by 20% as the temperature increasing from 200 K to 400 K.

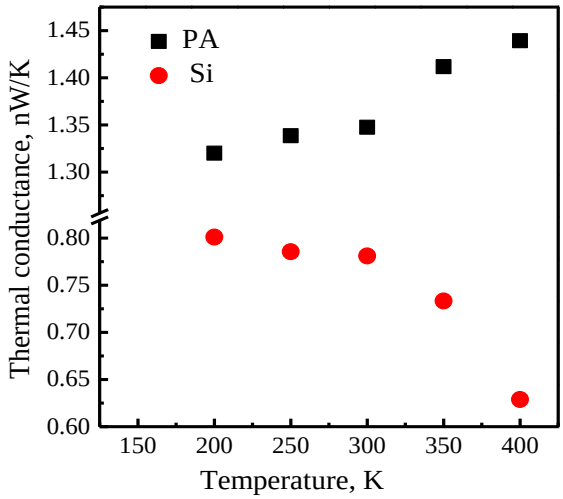

Figure S9. Temperature-dependent thermal conductance of PA and Si by MD simulations.

Figure S10 gives the temperature profiles of the two reversed heat fluxes in PA and Si. We can estimate that the average ΔT in PA and Si are about 40 K and 80 K, respectively. According to Fig. S10, the thermal conductance has a change of about 5% and 7.5% for PA and Si, respectively. So the thermal rectification ratio caused by temperature-dependent thermal conductance is about 6%.

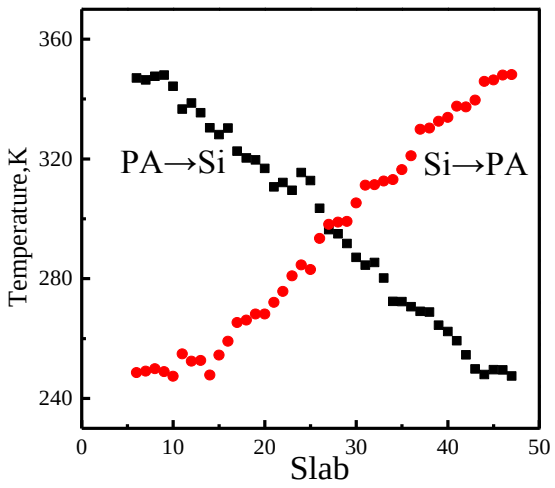

Figure S10. Temperature profiles of two reversed heat fluxes in PA and Si. The left side is PA and the right side is Si.